Received: 1 November 2023 | Revised: 23 February 2024 | Accepted: 4 March 2024

DOI: 10.1002/nano.202300166

RESEARCH ARTICLE

Nano Select WILEY

Pt-Fe loaded nanostructured silicon and improvement of the magnetic performance

Petra Granitzer[1] | **Klemens Rumpf**[1] | **Roberto Gonzalez-Rodriguez**[2] | **Jeffery L. Coffer**[3]

[1]Institute of Physics, University of Graz, Graz, Austria

[2]Department of Physics, University of North Texas, Denton, Texas, USA

[3]Department of Chemistry and Biochemistry, Texas Christian University, Fort Worth, Texas, USA

Correspondence
Petra Granitzer, Institute of Physics, University of Graz, Universitaetsplatz 5, 8010 Graz, Austria.
Email: petra.granitzer@uni-graz.at

Abstract

This work reports the pore-filling of porous silicon (PSi) and the loading of silicon nanotubes (SiNTs) with Pt-Fe nanoparticles (NPs) and the corresponding different magnetic behavior of the two composite systems. The fabrication of magnetic hard/soft nanostructures is in demand for the purpose of achieving both a high energy product as well as the replacement of rare earth permanent magnets. Pt-Fe templated by PSi shows a higher coercivity and remanence than SiNTs/Pt-Fe and thus a higher hard magnetic performance, the difference between coercivities being about 57%. Considering that the Pt-Fe deposits employ different molar ratios of Pt to Fe the coercivities vary in a range of 5% in the case of both template types. Comparing Pt-Fe loaded samples with Co-loaded samples in all cases, an increase of the coercivity and the remanence is observed for Pt-Fe, whereas in the case of PSi as template material the increase is significantly stronger (about twice as much) than in the case of SiNTs samples. Furthermore, the samples are investigated at high temperatures up to 950 K to determine the Curie temperature of the systems.

KEYWORDS

magnetic characterization, magnetic nanoparticles, porous silicon, PtFe, silicon nanotubes

1 | INTRODUCTION

The fabrication of self-organized semiconducting/ferromagnetic composite systems is of interest due to the silicon substrate material which renders it a promising candidate for magnetic on-chip applications. A further interesting applicability of such nanostructured materials could be the formation of permanent nanomagnets within quasi-regular pore- or tube arrangements. The self-organized formation of the nanostructured materials is of low cost as well as time-savings compared to lithographic methods. Different semiconductor templated morphologies are available, including porous silicon (PSi) as well as silicon nanotubes (SiNTs), each tunable in their inner diameter and also the distance between individual pores/tubes.[1,2] The tailorable morphology of the nanostructured silicon templates and the filling of these structures with magnetic materials of different geometry and size leads to tunable magnetic interactions between them as well. A decrease of the magnetic coupling between magnetic structures of adjacent pores with increasing interpore distance results in an increase of the magnetic anisotropy between easy and hard axis magnetization.[3] On the one hand magnetostatic coupling

between magnetic particles within the pores and between adjacent pores plays a crucial role[3]; on the other hand exchange coupling between, for example, bi-metal nanostructures is of importance and influences the performance of magnetic hard/soft nanostructures.[4] The combination of hard and soft magnetic materials resulting in hard/soft magnetic nanostructures are suitable to achieve a high energy product (BH_{max})[5] which increases with coercivity and remanence.[5] Soft magnetic materials offer a high saturation magnetization, a low anisotropy, and a small coercivity. Hard magnetic materials offer a moderate saturation magnetization and a high anisotropy.[6] The magnetic characteristics of the system strongly depend on the dimensions of the soft and the hard magnetic phase, whereas the soft magnetic should not exceed a critical size to ensure efficient exchange coupling showing a nearly rectangular hysteresis loop.[6] If the hard and the soft phase do not switch cooperatively a two-phase magnetic behavior is observed.[7] Combining hard/soft magnetic materials (Pt-Fe, Fe) can result in exchange coupling between the two phases and thus leading to high coercivities as well as high magnetic moments.[8] To achieve an energy product (BH_{max}) of the system as high as possible, the volume ratio of the two materials has to be optimized. Favorable are single domain particles which are thermally and magnetically stable which can be achieved by big enough particle sizes or exchange coupling between ferromagnetic/antiferromagnetic core-shell particles.[9] The magnetic properties are strongly dependent on the particle size and show below a certain size a superparamagnetic behavior when the thermal energy overcomes the energy barrier.[8]

In particular, face-centered cubic (fcc) Pt-Fe particles show a superparamagnetic or soft magnetic behavior depending on the size. In contrast, face-centered tetragonal (fct) Pt-Fe particles offer high uniaxial magnetocrystalline anisotropy with hard magnetic behavior.[4] Also exchange coupling of hard and soft magnetic particles can be exploited to enhance the coercivity and remanent magnetization.[10] The fabrication of Pt-Fe nanodot and antidot arrays by using anodic aluminum oxide (AAO) templates as a dry etching mask can serve as pinning sites and prevent domain wall motions thus leading to an enhancement of the coercivity.[11] Dipolar coupled hard and soft nanomagnets within mesoporous silica are used to produce structures with a magnetic behavior comparable to exchange coupled spring magnets although dipolar interactions are much weaker.[10] The fabrication of Pt-Fe particles is often performed by vacuum deposition techniques leading to a chemically disordered face-centered cubic structure with soft magnetic behavior.[12] To achieve the chemically ordered face-centered tetragonal structure thermally annealing is needed which can result in agglomeration of the particles.[8] A further approach to produce monodisperse particles is solution-phase synthesis[13] such as thermal decomposition of $Fe(CO)_5$ and reduction of $Pt(acac)_2$ in the presence of 1,2-alkanediol.[14]

Permanent magnets are mainly based on rare earth elements such as $Fe_{14}Nd_2B$ or $SmCo_5$. Rare earth elements are limited and expensive and thus there is an increased demand for alternatives.[15] Another approach is to use exchange coupled hard/soft magnetic materials with properties possibly overcoming the limitations of conventional permanent magnets.[6]

There are few reports on the investigation of Curie temperature (T_C) of nanocomposite systems as a function of grain structure, for example, it has been shown that T_C of a duplex phase alloy decreases with shorter intergranular space and with increasing grain size.[16] Also the dependence of T_C on the composition of nanocrystalline alloys has been investigated.[17]

This manuscript explores the magnetic properties of Pt-Fe-loaded composite materials formed within two different templates, PSi and SiNTs, which have potential in high-performance magnets and as rare earth magnet alternatives. While both Si nanoscale templates contain mesopores, their morphologies are quite different. PSi contains a dendritic morphology, with branching of the main vertical pore that offers different opportunities for metal nanoparticle templating than for the relatively vertical spaces offered by the Si nanotubes (Figure 1A,B). The sketch in Figure 1C demonstrates the loading of the two template materials with nanoparticles.

The aim here is explore differences between these two types of nanostructured Si in the subsequent creation of Pt-Fe phases which ideally offer hard magnetic behavior and thus a high coercivity. Exchange coupled hard/soft magnets are interesting for permanent magnet which were initially been proposed in the early 1990s.[18] One drawback is the necessary control of the size of the hard and the soft magnetic phase, with the dominant morphology being investigated thus far being thin films.[19]

It is found that PSi/Pt-Fe demonstrates superior hard magnetic behavior with a higher coercivity and remanence compared to SiNTs/Pt-Fe. Varying the Fe molar ratio in deposits results in a small coercivity range. Pt-Fe-loaded samples consistently show increased coercivity and remanence compared to Co-loaded samples, with PSi exhibiting a stronger effect compared to SiNTs. We also investigate here the T_C (i.e., the temperature above which a given material loses its ferromagnetic properties) of these systems up to 950 K, providing practical insights into their magnetic properties and potential applications.

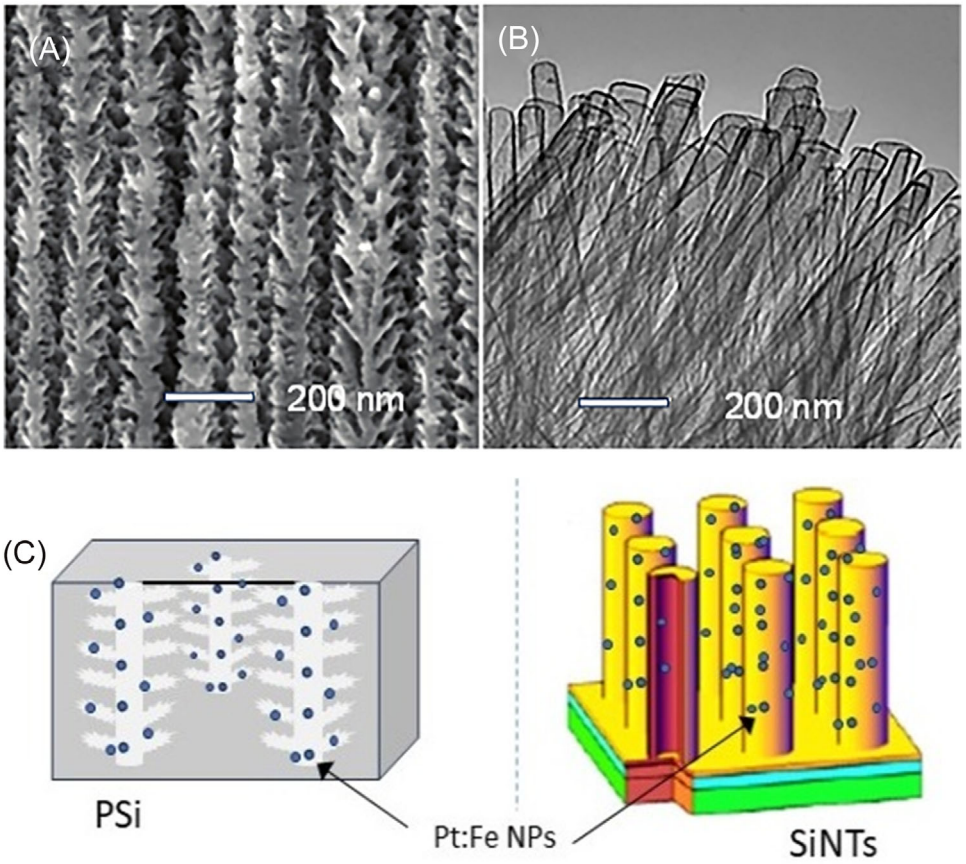

FIGURE 1 A, SEM image of anodized PSi and (B) TEM image of a SiNT array, illustrating the differences in morphology between the two types of Si templates. Scale bars are 200 nm. C, Sketch of Pt-Fe NPs loaded PSi and SiNTs.

2 | RESULTS AND DISCUSSION

The formation of Pt-Fe nanoparticles within nanostructured silicon is a multi-step process. The initial process consists of the SiNTs fabrication by using ZnO as a template, as described in the Experimental section. Once SiNTs were fabricated, surface functionalization was achieved using (3-aminopropyl)triethoxysilane (APTES) for the purpose of enhancing metal nanoparticle formation at the outer nanoparticle surface. In the case of porous silicon, the APTES functionalization was not necessary. Next, the growth of the Pt-Fe nanostructures was performed in a solution containing 0.1 mM citric acid, 0.5 mM H_2PtCl_6, and $Fe(NO_3)_3$. To determine the dependence of the magnetic properties on the precursor solution composition, the content of Pt precursor (chloroplatinic acid) was held constant while $Fe(NO_3)_3$ was varied between 0.5 and 3.0 mM. After an overnight soaking in the mixed metal ion solution, the samples were vacuum dried, followed by a 1-hour heat treatment in Ar atmosphere at 500°C, and finally washed with water and ethanol to remove any remaining physisorbed impurities.

In general, the magnetic properties of bi-metal nanoparticles are composition dependent. In the case of Pt-Fe growth the molar ratio of Pt:Fe was varied according to the ratios of 1:1, 1:3, and 1:6. In all three cases the average particle size is 5 nm, which can be seen in Figure 2D–F. Using PSi as template material the growth of Pt-Fe results in particles with an average size of 10 nm (Figure 2A–C).

It is desirable to achieve the $L1_0$ Pt-Fe phase, which is the hard magnetic one offering a high coercivity.[4] To determine magnetic characteristics, field dependent magnetization measurements have been performed for all samples, those templated by PSi as well as SiNTs with the three different molar ratios. Table 1 shows the coercivities that are dependent on the molar ratios.

The experimental molar ratios used to incorporate the Pt-Fe NPs into the SiNTs and PSi were 1:1, 1:3, and 1:6 for Pt:Fe, respectively. TEM energy dispersive x-ray analysis (EDX) for a given sample was used to probe metal content. The ratios of at% Pt to at% Fe for Pt:Fe in SiNTs were found to be 10.5, 2.0, and 0.5 for 1:1, 1:3, and 1:6, Pt:Fe respectively. For the case of at% Pt to at% Fe in Psi, the values are 29.0, 23.0, and 9.0, for 1:1, 1:3, and 1:6 of Pt:Fe,

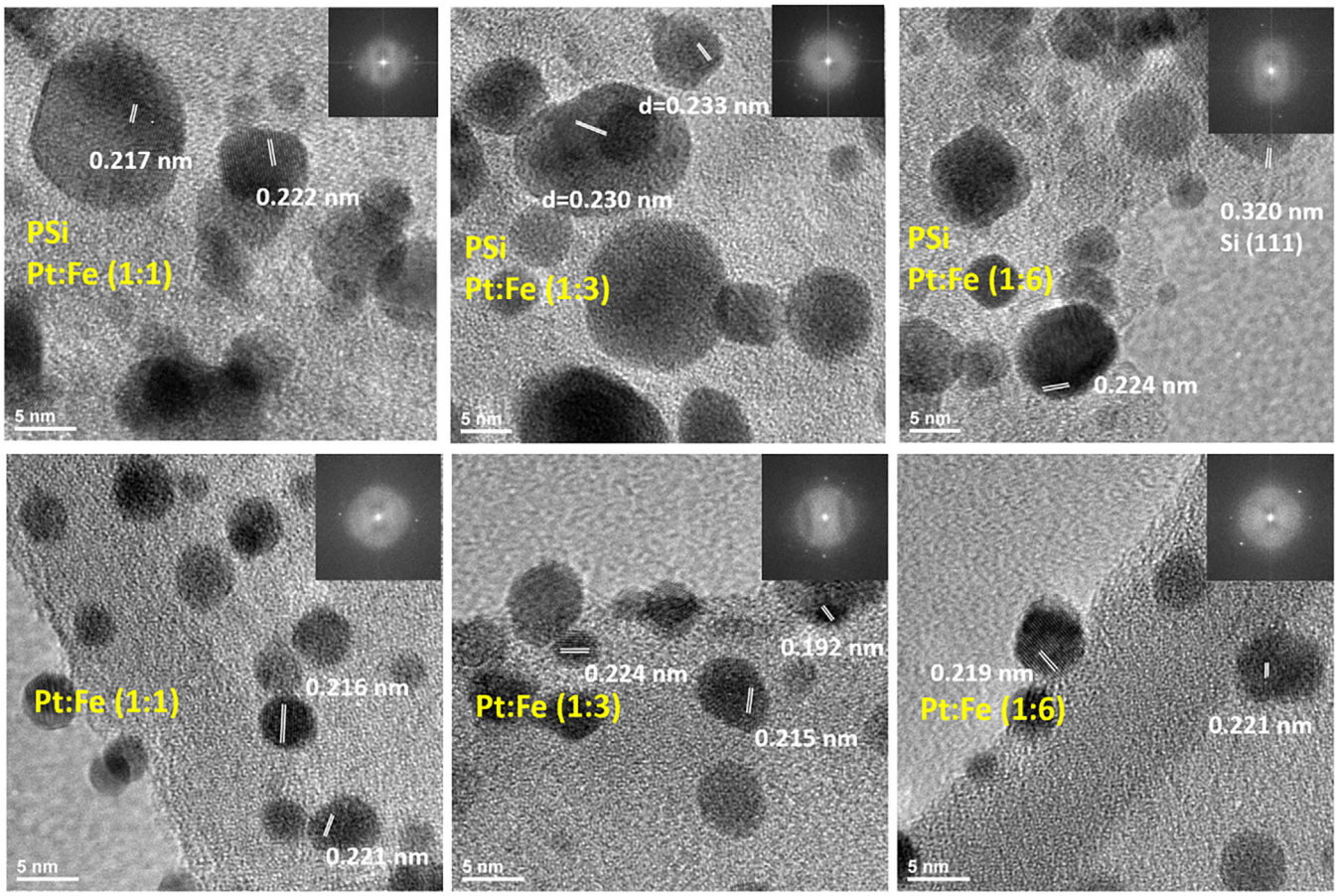

FIGURE 2 A–C, TEM image of Pt-Fe NPs grown within PSi offering an average particle size of 10 nm (A) molar ratio Pt:Fe 1:1, (B) molar ratio Pt:Fe 1:3, (C) molar ratio Pt:Fe 1:6, (D–F) TEM images of Pt-Fe particles grown within SiNTs offering an average size of 5 nm (D) molar ratio Pt:Fe 1:1; (E) molar ratio Pt:Fe 1:3; (F) molar ratio Pt:Fe (1:6).

TABLE 1 Coercivities (H_C) of PSi and SiNTs with embedded Pt-Fe NPs in dependence on the molar ratio of Pt:Fe measured at room temperature.

Magnetic material	PSi, H_C (Oe)	SiNTs, H_C (Oe)
Pt-Fe molar ratio Pt:Fe 1:1	530	228
Pt-Fe molar ratio Pt:Fe 1:3	545	232
Pt-Fe molar ratio Pt:Fe 1:6	560	240
Co particles	250	100

Note: For comparison the coercivities of Co-NPs loaded PSi and SiNTs are listed.

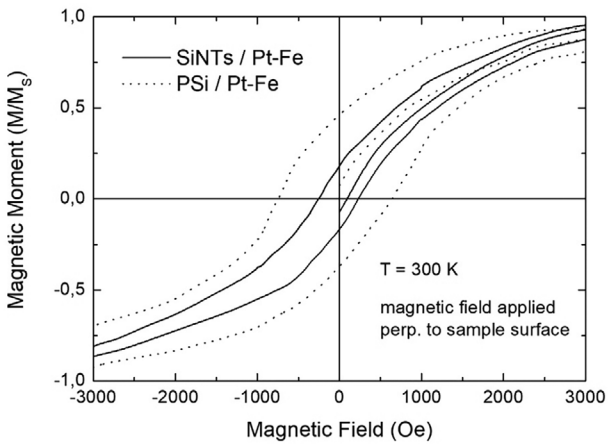

FIGURE 3 Field dependent magnetization curves of PSi (dotted line) and SiNTs (full line) loaded with Pt-Fe NPs.

respectively. Two points are abundantly clear from these measurements. First, given the large excess of Pt in many of these structures, Pt precipitates relatively fast in each type of nanostructured Si template. Second, the relative Pt content is higher in PSi templated samples than in SiNTs.

Magnetization measurements show that the coercivities of Pt-Fe NPs within PSi and SiNTs do not vary in a broad range (~5%) by varying the molar ratios. Furthermore the measurements show that the coercivities are about twice as high in using porous silicon as template material compared to SiNTs. Figure 3 shows the comparison of hysteresis curves between Pt-Fe grown within PSi and SiNTs. The variation of coercivities between the two sample-types is 57% at a Pt:Fe molar ratio of 1:6. The higher coercivities in using PSi as template can be explained by the bigger

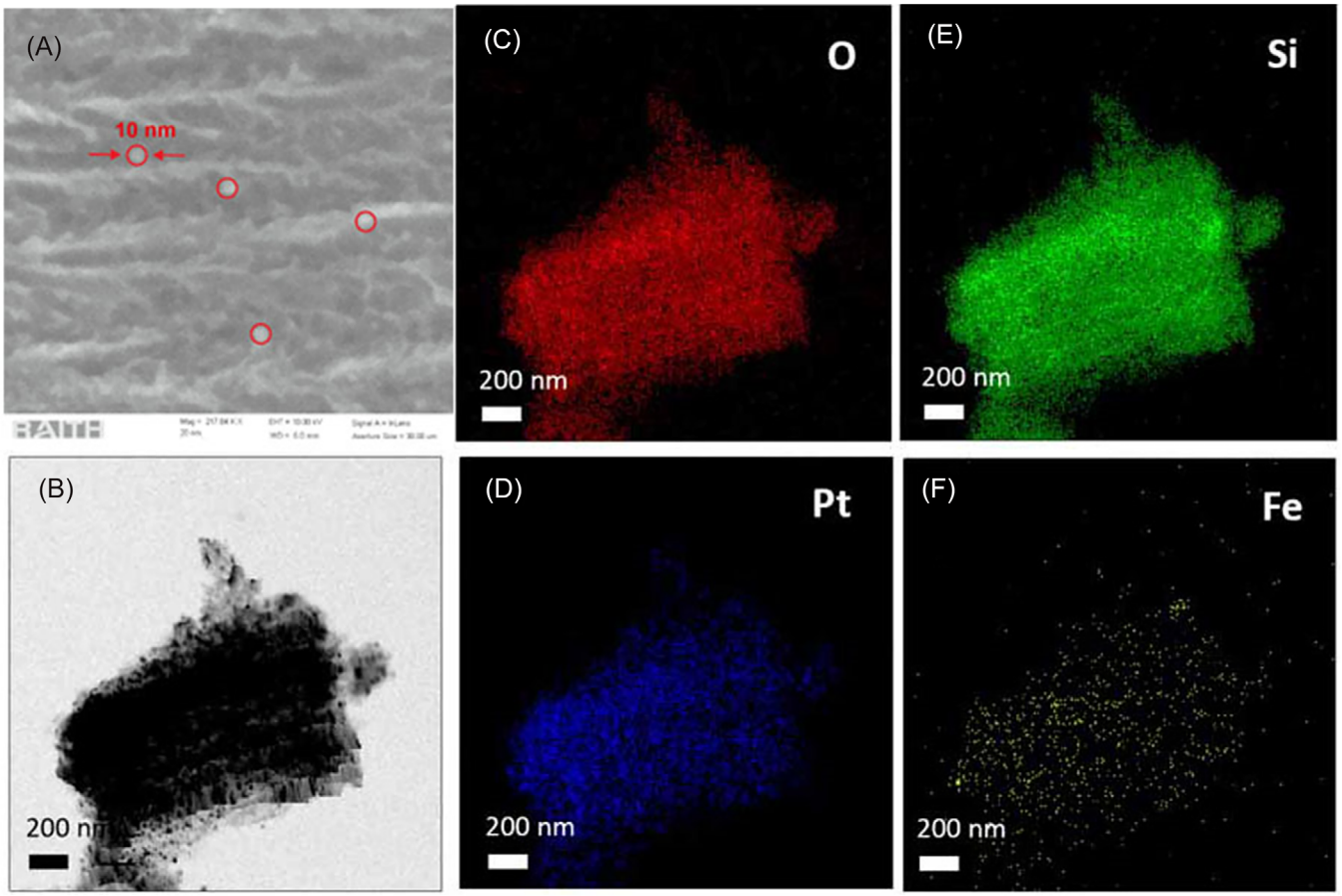

FIGURE 4 Cross-sectional SEM image (A) showing individual Pt-Fe NPs (encircled in red) within PSi and EDX mapping of a PSi-PtFe sample prepared from a Pt:Fe 1:6 ratio including the TEM image (B) of the sample as well as the oxygen (red) (C), platinum (blue) (D), silicon (green) (E), and iron (yellow) (F) distribution.

metal particle size, along with the likely metal nanoparticle separation brought about by the dendritic pore structure of PSi. The SEM image in Figure 4 exhibits individual PtFe particles within the pores with average size of 10 nm. Furthermore EDX maps show the oxygen, silicon, platinum, and iron distributions.

As mentioned before the aim of the work is to produce hard magnetic Pt-Fe NPs and so for comparison the magnetic behavior of Pt-Fe modified PSi and SiNTs with PSi and SiNTs samples loaded with cobalt (Co) particles (a known soft magnetic material) has been investigated. The magnetization measurements were performed at room temperature and show that the coercivities of Pt-Fe modified samples are always higher due to the harder magnetic behavior of Pt-Fe compared to the Co loaded samples. The last line in Table 1 shows the coercivity values of Co NPs loaded into PSi and SiNTs.

These results demonstrate that PSi used as template material offers in both cases, Pt-Fe and Co loading, a higher coercivity compared to the use of SiNTs. This reinforces the point made earlier regarding origins for this effect, namely bigger particle size of the metal deposits (Figure 1) as well as increased metal nanoparticle separation brought about by the dendritic pore structure of PSi. The particles do not strongly magnetically interact which can be seen from FORC (first order reversal curve) diagrams[20] (Figure 5). Detailed performance and interpretation of FORC measurements are reported in Vega et al. and Robert et al.[20,21] In the case of Pt-Fe deposited within SiNTs the particle size of 5 nm is in the superparamagnetic range and the low coercivities indicate the onset of superparamagnetism.[21,22]

Temperature dependent magnetization measurements have been performed in the range between 4.2 and 300 K showing the decrease of the coercivity which is a typical ferromagnetic property.[23] As example in Figure 6, the temperature dependency of the coercivity of Pt-Fe loaded SiNTs is depicted.

To determine the T_C of the two composite systems (Pt-Fe/SiNTs and Pt-Fe/PSi) magnetization measurements up to 950 K have been carried out. In both sample types the ratio Pt:Fe is 1:6. The temperature dependent magnetization of PSi with embedded Pt-Fe NPs is depicted in Figure 7 giving a T_C of 790 K. Figure 8A shows hysteresis curves

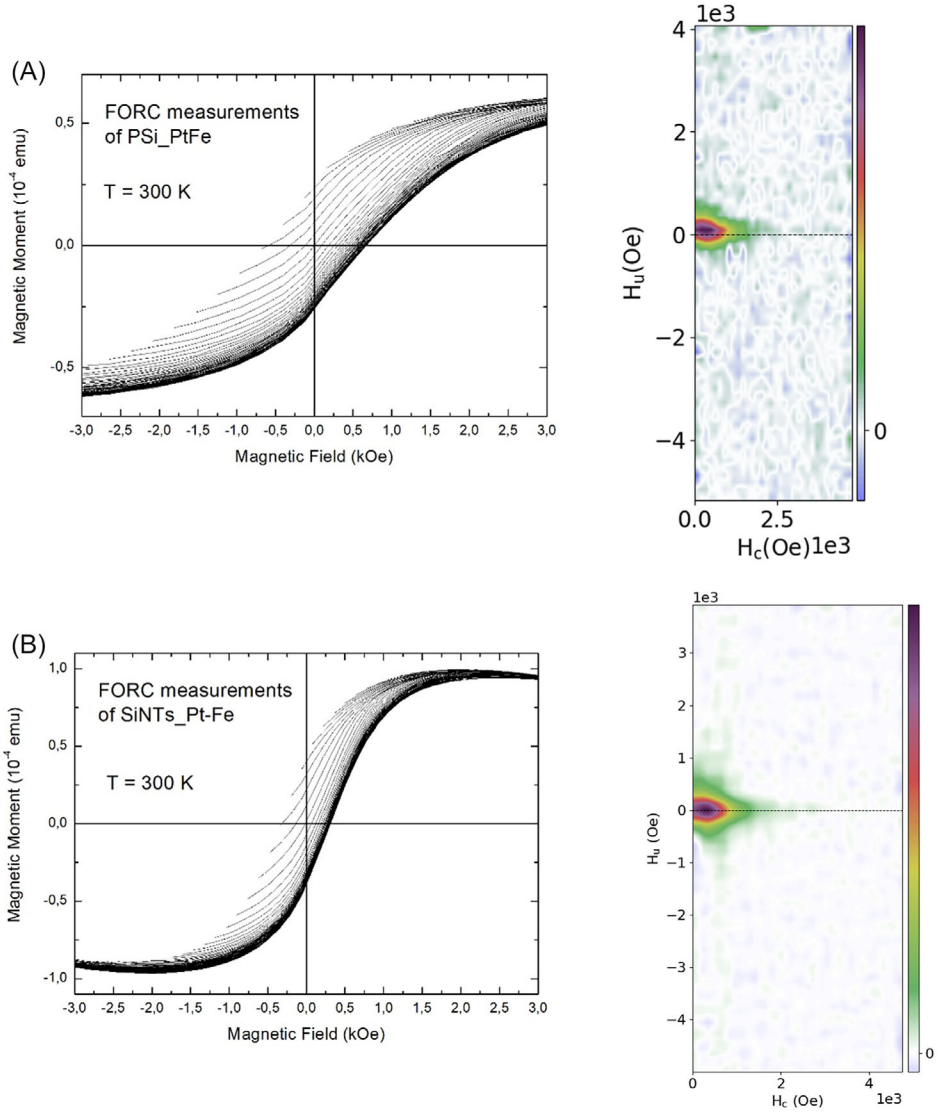

FIGURE 5 FORC measurements and corresponding diagrams of (A) Pt-Fe NPs within PSi and (B) Pt-Fe NPs within SiNTs showing that in both cases only very weak magnetic interaction is present.

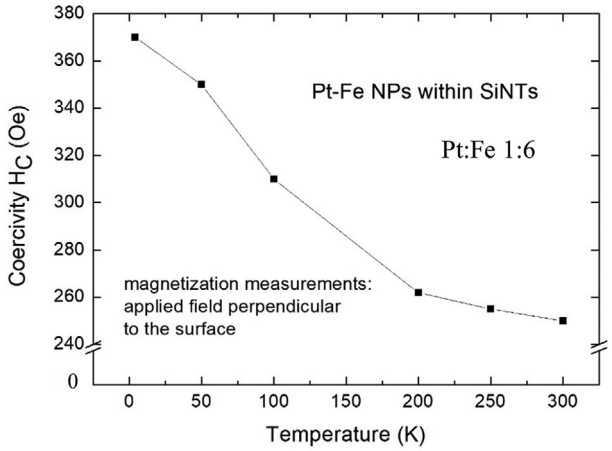

FIGURE 6 Temperature-dependent coercivity H_C of Pt-Fe loaded into SiNTs with a ratio Pt:Fe 1:6.

measured of Pt-Fe within SiNTs in a temperature range between 300 and 950 K. The curves indicate that the T_C is above 800 K and below 900 K. The temperature dependent measurements M(T) (Figure 8B) shows a T_C at 900 K. To determine T_C more precisely the inverse magnetic moment versus temperature has been depicted which also shows a T_C at 900 K. The different T_C of the two composite systems point out that T_C increases with decreasing particle size, since the Pt-Fe NPs grown within SiNTs offer an average size of 5 nm, whereas within PSi the average size is 10 nm.

3 | CONCLUSIONS

The varying magnetic response of the different composite systems templated by both porous silicon and silicon

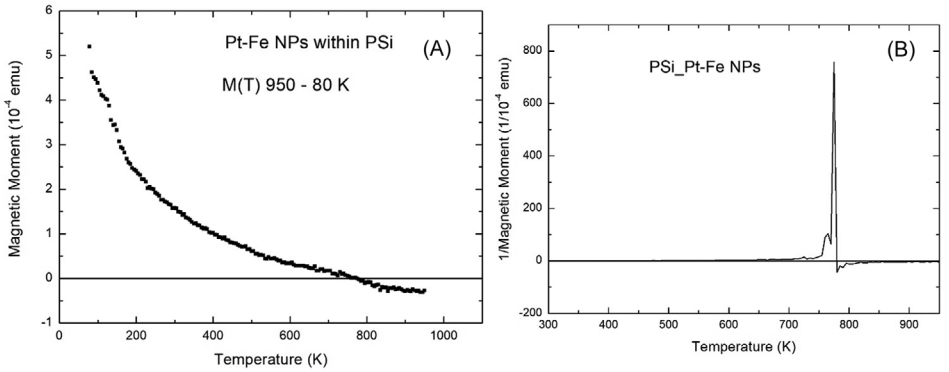

FIGURE 7 A, Temperature dependent magnetization measurement of PSi/Pt-Fe performed at $H = 20{,}000$ Oe. B, Inverse magnetic moment versus temperature to determine T_C, which is at 790 K.

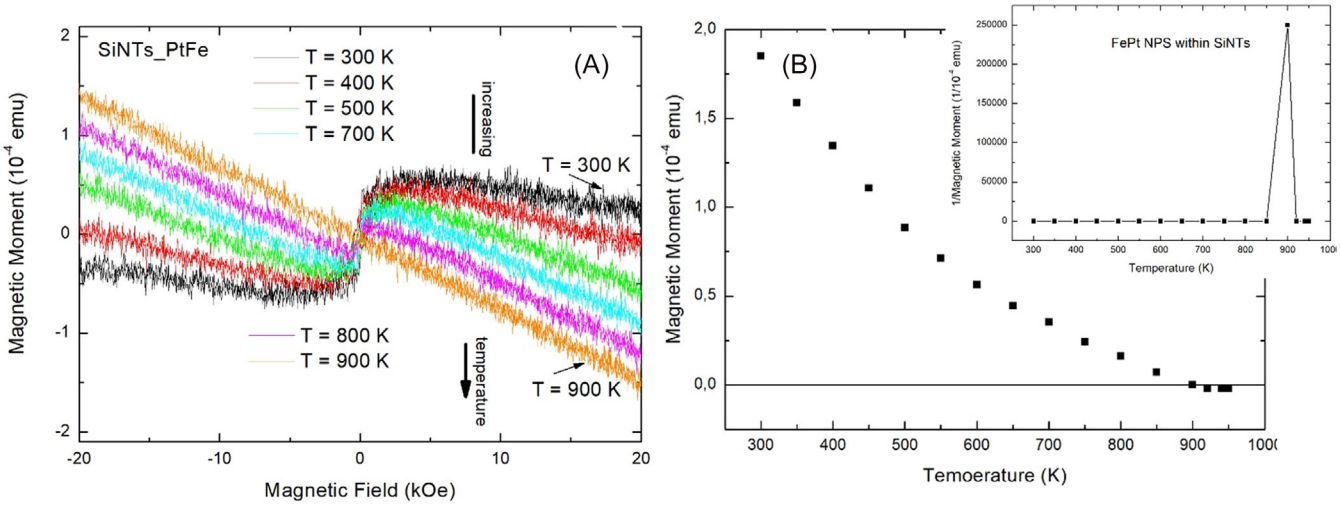

FIGURE 8 A, Field dependent magnetic measurements of Pt-Fe/SiNTs performed in a temperature range between 300 and 900 K show that T_C is between 800 and 900 K. B, Magnetization versus temperature between 300 and 950 K. The diamagnetic contribution has been considered. At 900 K the magnetization is vanished. The measurements have been performed at $H = 20000$ Oe. Inset: Inverse magnetic moment versus temperature to determine T_C, which is at 900 K.

nanotubes has been investigated as a function of Pt:Fe precursor composition. Overall PSi/Pt-Fe shows a higher coercivity and remanence than SiNTs/Pt-Fe and thus a higher hard magnetic performance. For a given Pt:Fe precursor ratio, the variation of the coercivities between SiNTs/Pt-Fe and PSi/Pt-Fe is about 57%.

Considering the Pt-Fe deposits prepared with different molar ratios of Pt to Fe, the coercivities vary in a range of 5% in the case of each template type. The magnitude of coercivity and of the remanence is always greater for Pt-Fe relative to Co for a given Si template, and in the case of PSi as template material the increase is stronger than in the case of SiNTs samples.

In addition to low temperature and room temperature magnetic measurements, the magnetic behavior of the samples has been investigated at high temperatures up to 950 K to determine T_C of the composite systems. T_C is lower for PSi loaded with Pt-Fe NPs which indicates that T_C increases with decreasing Pt-Fe particle size.

4 | EXPERIMENTAL SECTION

The porous silicon is produced by anodization of a highly doped n-type silicon wafer (0.01–0.013 Ω cm), with (1 0 0) orientation, polished on both sides in a 10 wt% HF solution, consisting of distilled water, 80% ethanol, and 48% HF. In using a current density of 75 mA cm^{-2} and an etching time of 8 min, the resulting morphology offers oriented, separated pores of about 50 nm in diameter, and a mean distance between the pores of 50 nm. The

thickness of the porous layer is about 40 μm. The morphological characteristics as pore diameter and inter-pore distance are determined by SEM in combination with image processing (samples in top view) and the thickness of the porous layer is determined by SEM of a cross-section of the sample. The SiNTs are fabricated using a packed array of ~1 μm long ZnO nanowires approximately 50 nm wide as a template with subsequent silicon deposition by CVD by using 0.5% SiH_4 99.5% UHP He as silicon precursor at a flow of 300 sccm, further diluted in a Helium (He) atmosphere at 510°C for 5 minutes, and finally, etching off the ZnO nanowires by using NH_4Cl in He at 500°C. The inner diameter of the tubes and the wall thickness can be tuned by the fabrication process, where the SiNTs inner diameter and length are given by the ZnO nanowires dimensions, and the shell thickness is tuned with the CVD conditions. For this study, we used Si NTs with inner diameter ~50 nm and ~10 nm in shell thickness. Pt-Fe nanoparticles (NPs) are deposited electroless using citric acid as a reducing agent inside the pores and the tubes, respectively, as the molar ratio of Pt to Fe is varied. For this purpose a three component solution consisting of 0.5 mM H_2PtCl_6, $Fe(NO_3)_3$, and 0.1 mM citric acid is used, whereas the concentration of $Fe(NO_3)_3$ is modified between 0.5 and 3.0 mM.

Growth of Co NPs within PSi and SiNTs is performed by a solution method. The PSi and Si NTs were immersed in a 10 mL methanol solution containing 0.2 g of $CoCl_2$ $6H_2O$ followed by a vacuum drying process overnight; then the samples were immersed in 10 mL of DI water and quickly added 0.1 g $NaBH_4$ under constant stirring. Finally, the samples are washed in DI and ethanol. Structural characterization was performed by using the transmission electron microscopy (TEM) JEOL JEM-2100.

CONFLICT OF INTEREST STATEMENT

The authors declare no conflict of interest.

DATA AVAILABILITY STATEMENT

Research data are not shared.

ORCID

Petra Granitzer https://orcid.org/0000-0002-7283-4392

REFERENCES

1. P. Granitzer, K. Rumpf, *Materials* **2010**, *3*, 943.
2. X. Huang, R. Gonzalez-Rodriguez, R. Rich, Z. Gryczynski, J. Coffer, *Chem. Commun.* **2013**, *49*, 5760.
3. K. Rumpf, P. Granitzer, N. Koshida, P. Poelt, M. Reissner, *Nanoscale Res. Lett.* **2014**, *9*, 412.
4. V. H. Le, S. H. Tolbert, *APL Mater.* **2014**, *2*, 113309.
5. R. Skomsky, J. M. D. Coey, *Phys. Rev. B* **1997**, *48*, 15812.
6. A. Lopez-Ortega, M. Estarder, G. Salazar-Alvarez, A. G. Roca, J. Nogues, *Phys. Rep.* **2015**, *553*, 1. https://doi.org/10.1016/j.physrep.2014.09.007
7. H. Zeng, J. Li, J. P. Liu, Z. L. Wang, S. Sun, *Nature* **2002**, *420*, 395.
8. S. Sun, *dv. Mater.* **2006**, *18*, 393.
9. H. C. Tong, C. Qian, L. Miloslavsky, S. Funada, X. Shi, F. Liu, S. Dey, *J. Magn. Magn. Mater.* **2000**, *209*, 56.
10. J. Li, Z. L. Wang, H. Zeng, S. H. Sun, J. P. Liu, *Appl. Phys. Lett.* **2003**, *82*, 3743.
11. C. H. Deng, M. Zhang, F. Wang, X. H. Xu, *J. Mag. Mag. Mater.* **2018**, *447*, 81.
12. R. A. Ristau, K. Barmak, L. H. Lewis, K. R. Coffey, J. K. Howard, *Appl. Phys.* **1999**, *86*, 4527.
13. D. L. Huber, *Small* **2005**, *1*, 482.
14. S. Sun, C. B. Murray, D. Weller, L. Folks, A. Moser, *Science.* **2000**, *287*, 1989.
15. O. Gutfleisch, M. A. Willard, E. Brück, C. H. Chen, S. G. Sankar, J. P. Liu, *Adv. Mater.* **2011**, *23*, 82
16. Y. Z. Shao, W. R. Zhong, G. M. Lin, X. D. Hu, *Int. J. Modern Phys. B.* **2007**, *21*, 4689. https://doi.org/10.1142/S0217979207038046
17. A. Hernando, I. Navarro, P. Gorria, *Phys. Rev. B.* **1995**, *51*, 3281.
18. E. F. Kneller, R. Hawig, *IEEE Trans. Magn.* **1991**, *27*, 3588.
19. A. Gayen, B. Biswas, A. K. Singh, P. Saravanan, A. Perumal, *Physics Proceda.* **2014**, *54*, 23.
20. V. Vega, W. O. Rosa, J. Garcia, T. Sanchez, J. D. Santos, F. Beron, K. R. Pirota, V. M. Prida, B. Hernando, *J. Nanosci. Nanotechnol.* **2012**, *12*, 4736.
21. A. P. Roberts, D. Heslop, X. Zhao, C. R. Pike, *Rev. Geophys.* **2014**, *52*, 557. https://doi.org/10.1002/2014RG000462
22. B. Rellinghaus, S. Steppert, M. Acet, E. F. Wassermann, *J. Mag. Mag. Mater.* **2003**, *266*, 142.
23. J. M. D. Coey, *Magnetism and Magnetic Materials*, Cambridge University Press **2012**.

How to cite this article: P. Granitzer, K. Rumpf, R. Gonzalez-Rodriguez, J. L. Coffer, *Nano Select* **2024**, *5*, 2300166.
https://doi.org/10.1002/nano.202300166